Inclusion of Neutral Points in Measurement-Based Frequency-Dependent Transformer Model

Bjørn Gustavsen, *Fellow*

***Abstract*—Measurement-based wide-band black-box transformer models are well suited for simulation studies of high-frequency transients in power systems. The inclusion of neutral points in such models can be difficult when the model is required to simulate voltage transfer to windings with high-impedance loads. The difficulty arises because it is then necessary to include the small winding capacitive currents in the measurement and model extraction procedure, while at the same time the capacitances can be asymmetrical with respect to the winding ends. This paper introduces a new measurement procedure which can accurately capture the effect of such capacitive asymmetries. The procedure is demonstrated for a wye-wye connected transformer. The measurement and subsequent passive rational modeling results in two alternative models. The first is a four-terminal model with bonded high-voltage and low-voltage terminals, suitable for simulation of lightning overvoltages in distribution systems. The second is a full eight-terminal model, suitable for general purpose transient studies.**

***Index Terms*—Transformer, neutral points, modeling, frequency dependent.**

I. Introduction

HIGH frequency transformer models are needed in simulation of transient overvoltages in power systems [1],[2]. These overvoltages result from lightning strokes, switching operations, fault situations or switch-mode power electronic converters. The model's accuracy requirement is in particular high when calculating voltages that appear on the transformer terminals, voltages that are transferred between voltage levels, and internal voltages that stress the transformer insulation.

Transformer internal voltage stresses can only be assessed using a detailed model of the transformer, i.e. by a so-called white box model [3]. Such models are usually calculated based on spatial discretization of the transformer windings, yielding a ladder-type RLCG network which can be cast as a state-space model for efficient inclusion in EMT simulation programs [4],[5]. White-box models can in practice only be created by the transformer manufacturer because the required knowledge about the geometry details is known only to the manufacturer.

In general studies of network transients it is sufficient to use a terminal equivalent of the transformer, also known as black-box model. For instance, in insulation co-ordination studies the transformer is often represented by a lumped capacitance to earth in each phase, or by lumped capacitances in combination with a 50/60 Hz transformer model [6]. Although such modeling can be sufficient in some studies, a more accurate modeling approach should be adopted when high accuracy is required.

One successful way of obtaining a high-accuracy terminal equivalent is via small-signal frequency sweep measurements of admittance, voltage transfer or scattering parameters [7]-[14]. The measurements are with these approaches subjected to approximation with rational functions that can be included in EMT simulation programs in the form of a lumped circuit equivalent or a state-space model.

One major challenge with the measurement-based approach is inclusion of the low-frequency capacitive behavior in transformers with one or more ungrounded windings (delta or ungrounded wye). This capacitive behavior is essential for simulating the transformer response with open or high-impedance terminations. The difficulty arises because the model must capture both the (large) short circuit currents and the (small) capacitive charging currents. For instance, with direct measurement of terminal (short-circuit) admittance matrix elements [9], these small capacitive currents tend to become lost in the measurement noise and the resulting data is unable to represent the voltage transfer to an open winding. This problem was overcome in [10] by introducing separate zero-sequence measurements that capture the capacitive behavior. One might think that the zero-sequence measurement approach can easily be extended to handle neutral points as terminals. It will be shown that such extension is not straightforward.

To observe the voltage in an open neutral point, the admittance model can be complemented with voltage transfer functions from the terminals to the neutral point [15]. However, if a component is to be connected to the neutral point (surge

Manuscript received… This work was supported by the consortium participants of the SINTEF-led projects “ProTrafo” (project no. 269303/E20) and "FastTrans" (project no. 294508/E20).

B. Gustavsen is with SINTEF Energy Research, N-7465 Trondheim, Norway (e-mail: bjorn.gustavsen@sintef.no).

This article has been accepted for publication in IEEE Transactions on Power Delivery. This is the author's version which has not been fully edited and content may change prior to final publication. Citation information: DOI 10.1109/TPWRD.2021.3098701

arrester, Petersen arc suppression coil,...) it becomes necessary to represent the neutral point(s) as terminal(s) in an extended admittance model.

This paper shows a new procedure for measurement of the transformer admittance matrix that permits to include the transformer neutral points as terminals. The approach is demonstrated for a wye-wye connected two-winding transformer. The main strategy is to perform an initial measurement with the high-voltage (HV) sides and low-voltage (LV) sides bonded, defining a 4×4 admittance system with the two neutral points included as terminals. As will be shown, a strong capacitive asymmetry exists with respect to the line end and neutral end of the transformer windings, thereby preventing the use of assumed matrix symmetries. For that reason the measurement setup in [9] is modified to utilize a wide-band injection transformer and voltage probes. By combining measurements using this setup, a very accurate 4×4 admittance matrix can be calculated. This matrix is afterwards combined with a measured 6×6 admittance matrix with respect to the six external terminals (with grounded neutral points) to obtain the full 8×8 matrix that includes the neutral points as terminals. This matrix is afterwards subjected to approximation with a high-order pole-residue model using existing fitting and passivity enforcement methods. The accuracy of the final model is validated by comparing measured time domain voltage responses with simulation results.

II. Problem Statement

The objective is to create a general measurement-based modeling approach for wye-wye connected transformers with inclusion of neutral points as terminals. The model is to include the transformer frequency-dependent effects over a wide range, from 50/60 Hz up to several MHz.

This work develops two models as shown in Fig. 1:

1. A four-terminal zero sequence model (with HV and LV terminals bonded).
2. A complete eight-terminal model.

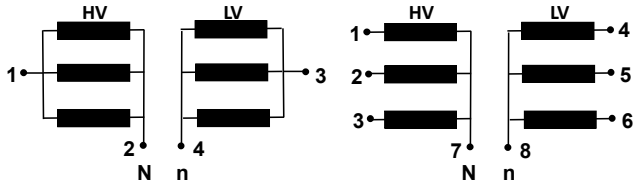

Fig. 1. Four-terminal model (left) and eight-terminal model (right).

The first model is suitable for representing distribution transformers in lightning overvoltage studies. The overvoltages are in such studies dominated by zero-sequence components due to phase-to-phase flashovers on overhead lines, implying that the voltages are fairly similar on the three phases. The second model is suitable for representing transformers in general transient calculations, e.g. switching overvoltage studies.

Both models are to be obtained starting from frequency sweep measurements that provide the transformer's terminal admittance matrix (4×4 or 8×8). The *n*-terminal admittance matrix $\mathbf{Y}$ is in both cases to be fitted with a stable and passive rational model on pole-residue form (1).

$$\mathbf{Y}^{n\times n}(\omega) = \mathbf{R}_0^{n\times n} + \sum_{i=1}^{N} \frac{\mathbf{R}_i^{n\times n}}{j\omega - a_i} \quad ,i = 1,\ldots,N \qquad (1)$$

III. Transformer

The considered transformer is a wye-wye connected 3-phase 300 kVA unit with nominal voltage ratio 11000:230 Volt. The HV windings are of layer type while the LV windings are foil type. This is the same unit used in the study of neutral point overvoltages in [15].

IV. Problems With Existing Measurement Methods

To see the challenges with the inclusion of neutral points, we consider the 4-terminal modeling in the left part of Fig. 1 using two existing approaches.

A. Direct Measurements

With the admittance measurement setup in [9], the elements of $\mathbf{Y}^{4\times4}$ are measured in a short-circuit condition, one-by-one. In such measurement, the (small) capacitive charging currents are lost in the (large) short-circuit currents towards lower frequencies. The inaccurate representation of the capacitive currents may cause highly inaccurate results in voltage transfer simulations when the HV or LV winding is ungrounded and connected to a high-impedance load [10].

B. Enforcement of Measured Common-Mode Behavior

The contribution from the capacitive currents can be represented more accurately by performing an additional common-mode admittance measurement as shown in Fig. 2. This gives a 2×2 matrix $\mathbf{Y}_{\text{comm}}$. This information must now be imposed on the original $\mathbf{Y}^{4\times4}$ which is obtained using direct measurements. A generalization of the zero-sequence measurement approach in [10] leads to the following approach.

For each 2×2 block i, j of $\mathbf{Y}^{4\times4}$, perform these operations:

1. Subtract from each row the average of the row sum.
2. Subtract from each column the average of the column sum.
3. Add to all elements the value $\mathbf{Y}_{\text{comm}}(i, j)/4$.

The modified matrix $\tilde{\mathbf{Y}}^{4\times4}$ now gets exactly the common-mode behavior defined by $\mathbf{Y}_{\text{comm}}$. This procedure assumes a certain symmetry, namely that $i_{1,A} = i_{1,B}$ and $i_{2,A} = i_{2,B}$ in Fig. 2.

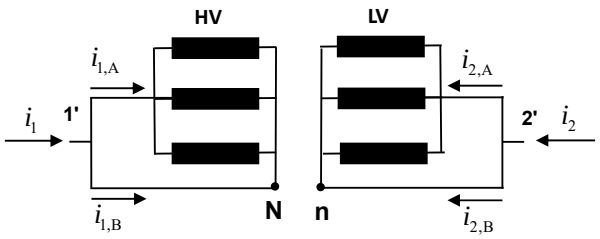

Fig. 2. Common-mode measurement and low-frequency current distribution.

C. Measured Results

The two measurement approaches are applied to the

This article has been accepted for publication in IEEE Transactions on Power Delivery. This is the author's version which has not been fully edited and content may change prior to final publication. Citation information: DOI 10.1109/TPWRD.2021.3098701

transformer described in Section III. Fig. 3 shows the eigenvalues of the obtained $\mathbf{Y}^{4\times4}$ and $\tilde{\mathbf{Y}}^{4\times4}$. It is observed that with the direct measurement approach, the two small eigenvalues are not complying with the expected low-frequency capacitive behavior which is a straight line, $y = j\omega C$. When including the common-mode measurements, the expected low frequency capacitive behavior is obtained.

Fig. 4 shows the voltage transfer from high to low with terminals 3 and 4 ungrounded, calculated from $\mathbf{Y}^{4\times4}$ and from $\tilde{\mathbf{Y}}^{4\times4}$. This 2×2 voltage transfer $\mathbf{H}_{\text{openLV}}$ is calculated by (2) from the lower partitioning of $\mathbf{Y}^{4\times4}$ (or $\tilde{\mathbf{Y}}^{4\times4}$) in (3). The expression (2) results by imposing that the LV side current is zero in the admittance matrix definition $\mathbf{i} = \mathbf{Y}\mathbf{v}$. This gives $\mathbf{0} = \mathbf{C}\mathbf{v}_H + \mathbf{D}\mathbf{v}_L$ so that $\mathbf{v}_L = -\mathbf{D}^{-1}\mathbf{C}\mathbf{v}_H$.

$$\mathbf{H}_{\text{openLV}} = -\mathbf{D}^{-1}\mathbf{C} \tag{2}$$

$$\mathbf{Y}^{4\times4} = \begin{bmatrix} \mathbf{A} & \mathbf{B} \\ \mathbf{C} & \mathbf{D} \end{bmatrix} \tag{3}$$

The calculated voltage transfer in Fig. 4 is compared with a voltage transfer measurement using voltage probes. It can be observed that neither of the matrices $\mathbf{Y}^{4\times4}$ or $\tilde{\mathbf{Y}}^{4\times4}$ give an acceptable result for the calculated low-frequency voltage transfer.

The reason why $\mathbf{Y}^{4\times4}$ gives an inaccurate result is that its two small eigenvalues are inaccurate below 200 kHz. These eigenvalues are associated with capacitive currents which represent the effect of capacitive coupling between windings, and between windings and earth. Without a correct representation of these capacitive couplings, errors will result in calculations of transferred voltage to a winding whose neutral point is ungrounded and terminals are open-ended or connected to a high-impedance load.

The reason why also $\tilde{\mathbf{Y}}^{4\times4}$ gives a poor result can be explained as follows. The given transformer has a HV layer-type winding with multiple layers. Fig. 5 illustrates the main capacitive elements for such transformer. Only the line-end layer of the HV winding has a substantial capacitive coupling to the LV winding while only the neutral-end layer has a substantial capacitive coupling to earth. Therefore, applying a voltage to the HV line end with the N-point grounded will give a higher voltage coupled to the LV winding than application of a voltage to the HV N-point with the line end grounded. This asymmetry in capacitive coupling from the HV winding ends to the LV winding (and to earth) is not compliant with the assumed common-mode current distribution $i_{1,A} = i_{1,B}$ and $i_{2,A} = i_{2,B}$ in Fig. 2 that was assumed when calculating $\tilde{\mathbf{Y}}^{4\times4}$.

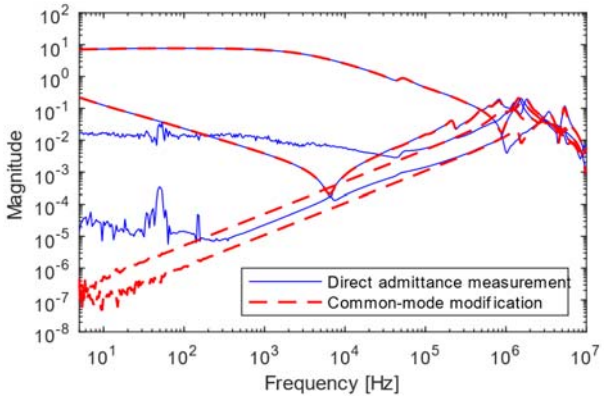

Fig. 3. Eigenvalues of $\mathbf{Y}^{4\times4}$.

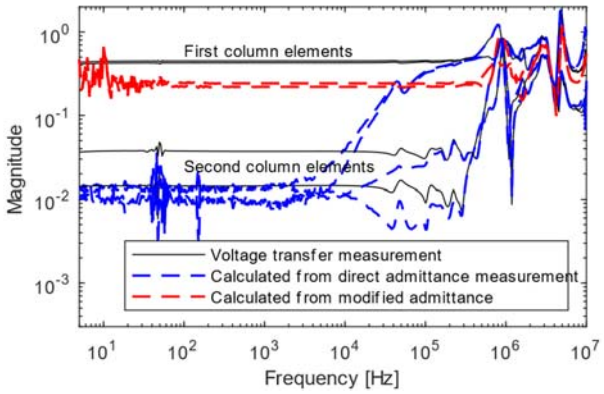

Fig. 4. Voltage transfer from HV winding terminals to LV winding terminals.

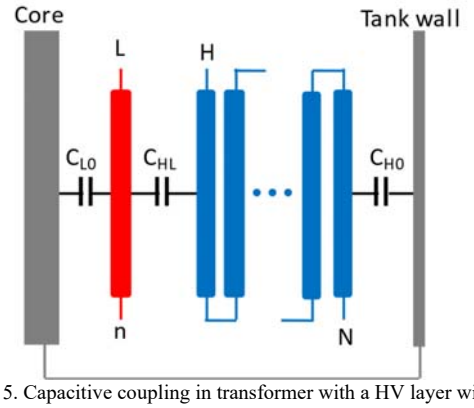

Fig. 5. Capacitive coupling in transformer with a HV layer winding.

V. Four-Terminal Measurements and Modeling

A new measurement procedure is introduced which is capable of properly representing the capacitive currents, including the effect of capacitive asymmetries between windings and between windings and earth. Terminal numbering is according to the left panel of Fig. 1.

A. Instrumentation

The measurement procedure makes use of a vector network analyzer and a measurement box with built-in current sensor, similar to [9]. In addition, it is necessary to use two passive voltage probes in combination with a wide-band injection (separation) transformer, see Table I.

This article has been accepted for publication in IEEE Transactions on Power Delivery. This is the author's version which has not been fully edited and content may change prior to final publication. Citation information: DOI 10.1109/TPWRD.2021.3098701

TABLE I.
LIST OF INSTRUMENTS.

Vector network analyzer	Agilent E5061B-3L5
Current sensor	Ion Physics, model CM-100-6L
Voltage probes (two of)	10 MΩ, passive type
Injection transformer	Omicron B-WIT-100 (1 Hz-10 MHz)

B. *Measuring Diagonal Blocks*

The following shows the measurements for establishing diagonal block **A** in (3). The procedure for measuring **D** is similar.

The information about capacitive asymmetries is captured by the differential mode measurement in the left part of Fig. 6. The use of the injection transformer prevents the HV winding from having a direct connection to ground. Therefore, the HV winding attains a potential which is shifted with respect to ground when the transformer has internal capacitive asymmetries. This potential shift information is captured by measurement of voltage transfer functions $h_1 = v_1 / v_m$ and $h_2 = v_2 / v_m$ (using voltage probes), in addition to the differential-mode admittance $y_m^{\text{diff}} = i_m / v_m$.

The sum of elements in **A** is obtained by the common-mode measurement in the right panel of Fig. 6, obtained as $y_m^{\text{comm}} = i_m / v_m$.

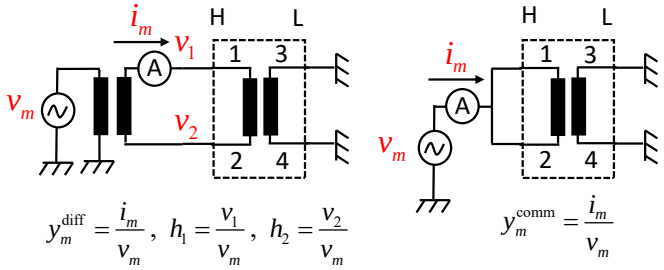

Fig. 6. Differential-mode (left) and common-mode-mode (right) measurement.

From the measurements and the admittance matrix definition $\mathbf{i} = \mathbf{Y}\mathbf{v}$, one can establish (4a), (4b) and (4c)

$$y_m^{\text{diff}} = \frac{i_m}{v_m} = \frac{1}{v_m}(y_{11}v_1 + y_{12}v_2) = y_{11}h_1 + y_{12}h_2 \qquad (4a)$$

$$-y_m^{\text{diff}} = \frac{-i_m}{v_m} = \frac{1}{v_m}(y_{21}v_1 + y_{22}v_2) = y_{21}h_1 + y_{22}h_2 \qquad (4b)$$

$$y_m^{\text{comm}} = \frac{i_m}{v_m} = y_{11} + y_{12} + y_{21} + y_{22} \qquad (4c)$$

which permit to establish (5) for calculating the admittance matrix elements when symmetry $y_{21} = y_{12}$ is utilized.

$$\begin{bmatrix} h_1 & h_2 & 0 \\ 0 & h_1 & h_2 \\ 1 & 2 & 1 \end{bmatrix} \cdot \begin{bmatrix} y_{11} \\ y_{12} \\ y_{22} \end{bmatrix} = \begin{bmatrix} y_m^{\text{diff}} \\ -y_m^{\text{diff}} \\ y_m^{\text{comm}} \end{bmatrix} \qquad (5)$$

Fig. 7a shows the measured elements of y_m^{comm} and y_m^{diff}. As expected, the common-mode admittance element is small at low frequencies while the differential mode element is large.

Fig. 7b shows the measured voltage transfer functions h_1 and h_2. It is observed that they are very different in magnitude, which is a result of the transformer internal capacitive asymmetry.

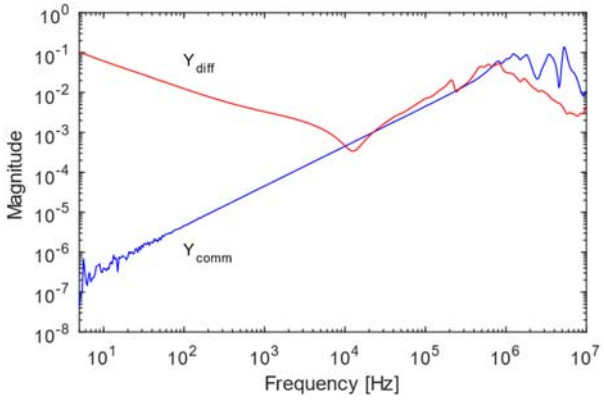

Fig. 7a. Common-mode and differential-mode admittance.

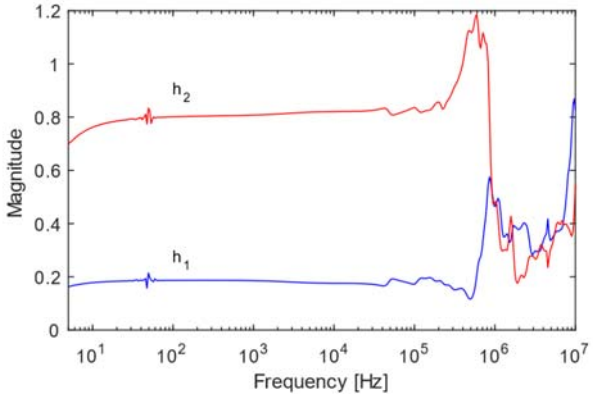

Fig. 7b. Voltage transfer functions h_1 and h_2.

The observed noise in the responses at lower frequencies in Figs. 7a and 7b is removed below 5 kHz. This is achieved by replacing the frequency response of y_m^{comm} (below 5 kHz) by a capacitive behavior $y = j\omega C$, and by replacing y_m^{diff}, h_1 and h_2 with low-order rational approximations.

Figs. 8a and 8b show respectively the elements and eigenvalues of the calculated **A**. It is observed that the expected capacitive (linear) behavior of the small eigenvalue is well represented.

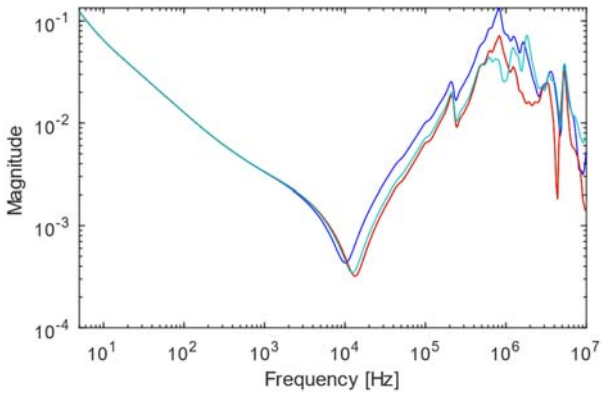

Fig. 8a. Elements of **A**.

This article has been accepted for publication in IEEE Transactions on Power Delivery. This is the author's version which has not been fully edited and content may change prior to final publication. Citation information: DOI 10.1109/TPWRD.2021.3098701

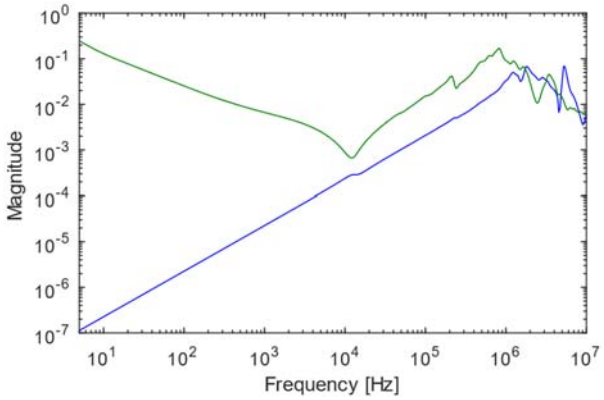

Fig. 8b. Eigenvalues of **A**.

C. Measuring Off-Diagonal Blocks

The measurements for establishing off-diagonal block **C** in (3) are presented next. This block is unsymmetrical so that four independent measurements are needed. In order to represent the unsymmetric capacitive coupling from the HV winding to the LV winding, it is necessary that a common-mode voltage application on the HV winding gives the correct (capacitive) current flowing from the LV terminals to ground when the LV terminals are grounded. This requirement implies that the row-sum is accurately measured for both rows of **C**. Similarly, both row-sums of **B** must be accurately measured to represent the capacitive coupling from the LV winding to the HV winding. The latter requirement implies that both column-sums of **C** must be accurate, since $\mathbf{B}=\mathbf{C}^T$.

To achieve the aforementioned requirements, a procedure is adopted which measures one element y_a, the matrix-sum y_b, one row-sum y_c, and one column-sum y_d. The associated admittance measurements y_a, y_b, y_c, y_d together with the related matrix operations lead to a matrix-vector equation (6) from which the elements of **C** are calculated.

$$\begin{bmatrix} 1 & 0 & 0 & 0 \\ 1 & 1 & 1 & 1 \\ 1 & 1 & 0 & 0 \\ 1 & 0 & 1 & 0 \end{bmatrix} \cdot \begin{bmatrix} C_{11} \\ C_{12} \\ C_{21} \\ C_{22} \end{bmatrix} = \begin{bmatrix} y_a \\ y_b \\ y_c \\ y_d \end{bmatrix} \tag{6}$$

It follows that the measurement of the matrix-sum in addition to the first row-sum and column-sum will ensure that also the second row-sum and column-sum will be accurate. Similarly, the measurement of the single element in addition to the associated row-sum and column-sum will ensure that also the second element in that row and column will be accurate.

The actual measurements are performed as follows.

Fig. 9a shows in the left panel the measurement of element $C_{11} = Y_{31}^{4\times4}$ and in the right panel the measurement of the matrix-sum of **C**.

Fig. 9b shows in the left panel the measurement of the first row-sum of **C**. The right panel shows the measurement of the first row-sum of **B**, which by definition is equal to the first column-sum of **C**.

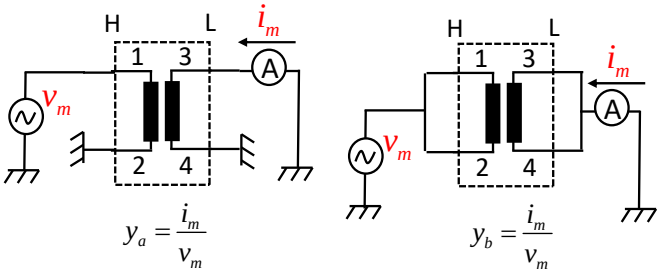

Fig. 9a. Measuring C_{11} (left) and sum of elements of **C** (right).

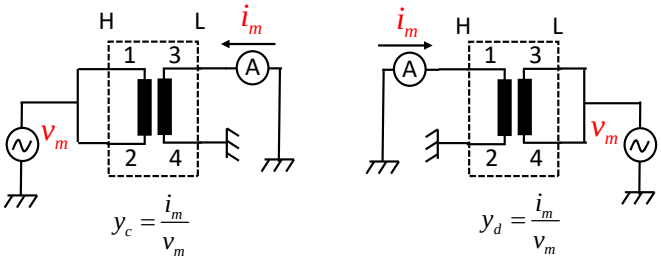

Fig. 9b. Measuring sum of elements in first row of **C** (left), and sum of elements in first row of **B** (right).

The low-frequency noise is removed from the four measurements, similarly as for **A**. Figs. 10a, 10b and 10c show respectively the measured elements y_a, y_b, y_c, y_d, the calculated elements of **C**, and the eigenvalues of **C**. Finally, **B** is established as $\mathbf{B}=\mathbf{C}^T$.

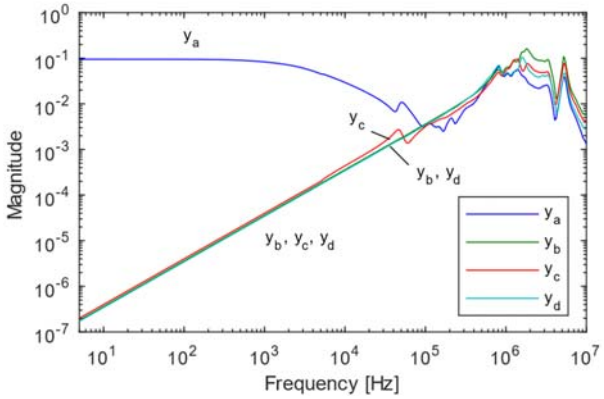

Fig. 10a. Measured quantities y_a, y_b, y_c, y_d.

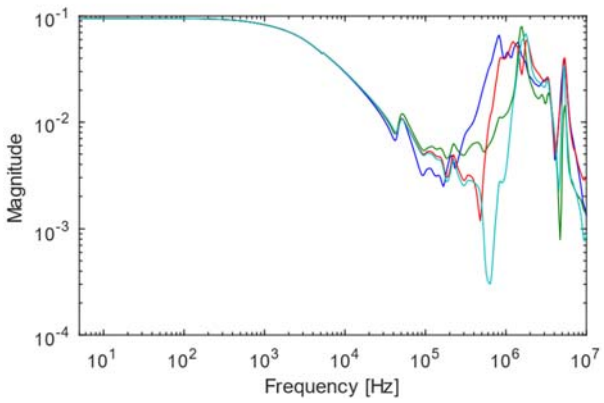

Fig. 10b. Elements of **C**.

This article has been accepted for publication in IEEE Transactions on Power Delivery. This is the author's version which has not been fully edited and content may change prior to final publication. Citation information: DOI 10.1109/TPWRD.2021.3098701

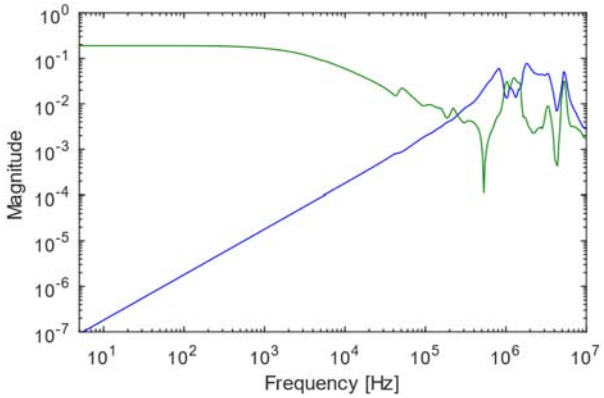

Fig. 10c. Eigenvalues of **C**.

D. Frequency Domain Validation

Fig. 11 shows the voltage transfer from the HV side to the LV side, calculated from the established admittance matrix by (2). The agreement with the measured voltage transfer function is clearly much better than in Fig. 5 where two existing measurement approaches were used.

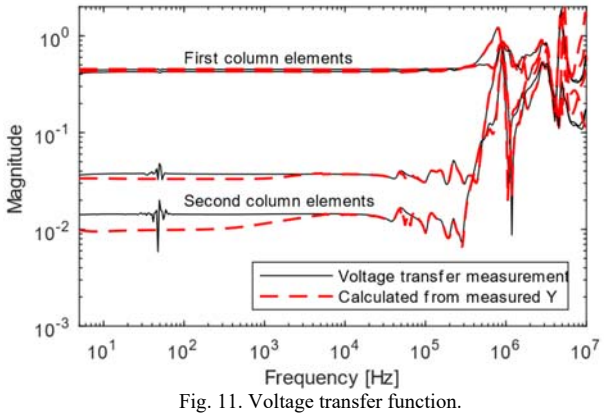

Fig. 11. Voltage transfer function.

E. Elimination of Measurement Cables

Finally, the impact of measurement cables (3-meter length) are eliminated from the obtained **Y** using the transmission line method described in in [16]. In this case, the transmission line admittance model of each cable is established via the cable data sheet per-unit-length parameters.

F. Model Extraction

A pole-residue model (1) is fitted to $\mathbf{Y}^{4\times4}(\omega)$ using well-established methods as outlined in Fig. 12. $\mathbf{Y}^{4\times4}(\omega)$ is first subjected to mode-revealing transformation (MRT) [17] by a passivity-preserving orthogonal matrix **Q**, making the small eigenvalues of $\mathbf{Y}^{4\times4}(\omega)$ more observable in the matrix elements. The transformed matrix $\hat{\mathbf{Y}}^{4\times4}(\omega)$ is approximated with a 60th order pole-residue model using vector fitting [18] with relaxation [19] and fast implementation [20]. The model is subjected to passivity enforcement by residue perturbation [21] with the fast implementation in [22] (RP-NNLS). The perturbed model is finally transformed back by applying the inverse MRT to the individual residue matrices $\hat{\mathbf{R}}_i^{4\times4}(\omega)$.

1. Transformation of data by MRT

$$\hat{\mathbf{Y}}^{4\times4}(\omega_k) = \mathbf{Q}^T\,\mathbf{Y}^{4\times4}(\omega_k)\,\mathbf{Q}\ ,k=1,2,...,K$$

2. Rational function approximation by Vector Fitting

$$\hat{\mathbf{Y}}^{4\times4}(\omega_k) \approx \hat{\mathbf{R}}_0^{4\times4} + \sum_{i=1}^{N}\frac{\hat{\mathbf{R}}_i^{4\times4}}{j\omega_k - a_i}\ ,k=1,...,K$$

3. Passivity enforcement by RP-NNLS

$$\hat{\mathbf{R}}_0^{4\times4} + \sum_{i=1}^{N}\frac{\hat{\mathbf{R}}_i^{4\times4}}{j\omega - a_i} \leftarrow (\hat{\mathbf{R}}_0^{4\times4} + \Delta\hat{\mathbf{R}}_0^{4\times4}) + \sum_{i=1}^{N}\frac{\hat{\mathbf{R}}_i^{4\times4} + \Delta\tilde{\mathbf{R}}_i^{4\times4}}{j\omega - a_i}$$

4. Back-transformation of perturbed model by inverse MRT

$$\mathbf{R}_i^{4\times4} = \mathbf{Q}\,\hat{\mathbf{R}}_i^{4\times4}\,\mathbf{Q}^T\ ,i=0,1,...,N$$

Fig. 12. Model extraction procedure.

Figs. 13 and 14 compare the eigenvalues and elements of $\mathbf{Y}^{4\times4}(\omega)$ of the original data with those of the pole-residue model. The accuracy of the model extraction is seen to be good, although it tends to deteriorate at very high frequencies as can be observed in Fig. 14.

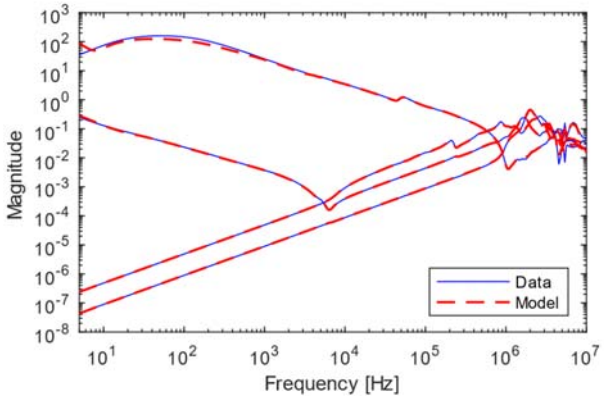

Fig. 13. Eigenvalues of $\mathbf{Y}^{4\times4}$.

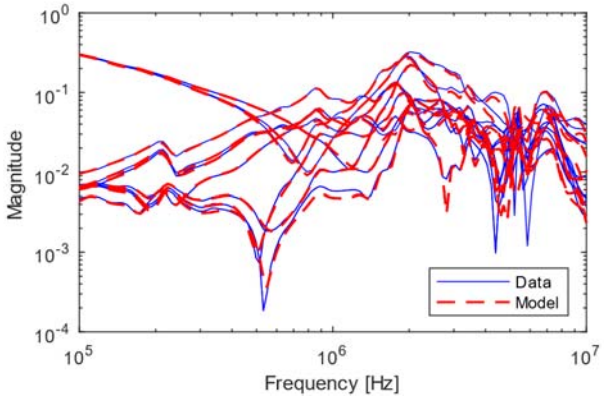

Fig. 14. Elements of $\mathbf{Y}^{4\times4}$ at high frequencies.

G. Time Domain Validation

The accuracy of the model is demonstrated by comparison with measured time domain step voltage responses. All measurements are performed directly on the transformer terminals. The test is performed with the voltage excitation on

This article has been accepted for publication in IEEE Transactions on Power Delivery. This is the author's version which has not been fully edited and content may change prior to final publication. Citation information: DOI 10.1109/TPWRD.2021.3098701

the HV side, on terminal 1 and on terminal 2 with the LV-side terminals open, see Fig. 15. The measured voltage on the excited terminal is applied to the model as an ideal voltage source.

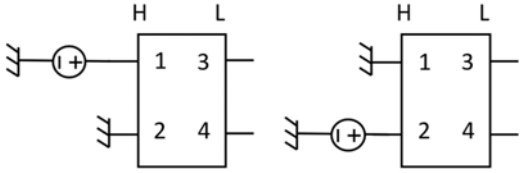

Fig. 15. Voltage excitations on HV side with open LV side.

Fig. 16 shows the voltage responses with the excitation on terminal 1. It is observed that the simulated voltages by the proposed model are in excellent agreement with the measured voltages on terminals 3 and 4.

Fig. 17 shows the voltage responses with the excitation on terminal 2. The model gives again a very good representation of the voltage on terminals 3 and 4. It is observed that the semi-stationary voltage on the LV-side terminals is now much lower than in Fig. 16. This change in transferred voltage is a result of the difference in capacitive coupling between the HV and LV windings, as seen from the line end and neutral end of the windings.

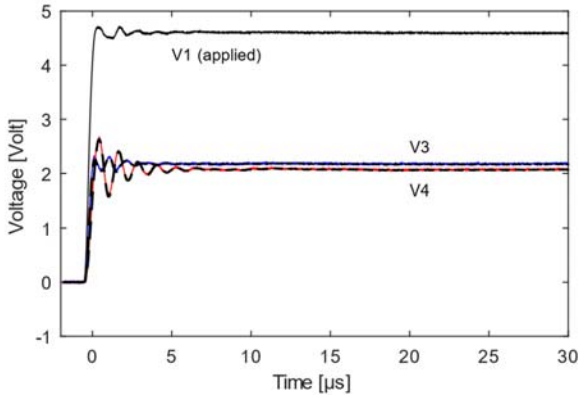

Fig. 16. Measured (solid traces) and simulated voltages (dashed traces).

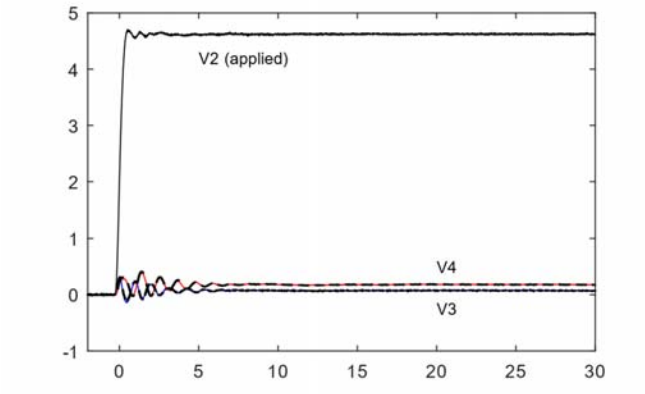

Fig. 17. Measured (solid traces) and simulated voltages (dashed traces).

For comparison, the same modeling procedure was applied with the admittance matrix obtained via the two existing measurement methods described in Sections IV.A and IV.B. Fig. 18 shows the simulation result corresponding to Fig. 16, i.e. excitation on terminal 1. It is observed that both methods give an unacceptable result. The poor agreement is to be expected as this example corresponds directly to the first column of the voltage transfer function in Fig. 4, where both methods give an inaccurate result.

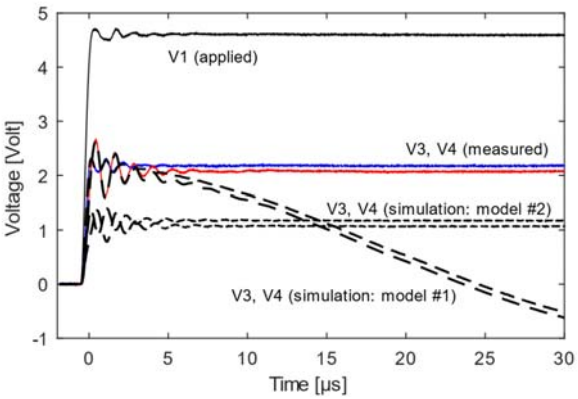

Fig. 18. Model extracted from **Y** when obtained via existing measurement methods. Model #1: Direct admittance measurement; Model #2: modified via common-mode measurements.

VI. Eight-Terminal Measurements And Modeling

A. Overview

The situation is now considered that a complete model of the transformer is required, with inclusion of the neutral points in addition to the six phase terminals. To achieve this, the already measured $\mathbf{Y}^{4\times4}$ is combined with a six-terminal measurement $\mathbf{Y}^{6\times6}$ where both neutral points are grounded on the transformer.

To better show the procedure, the terminals in the 4×4 measurement are renumbered as shown in the left part of Fig. 19. The renumbering amounts to an interchange of matrix rows and columns, giving a new matrix $\tilde{\mathbf{Y}}^{4\times4}$.

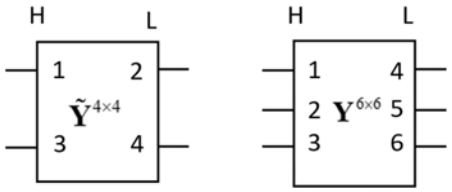

Fig. 19. Terminal numbering for $\tilde{\mathbf{Y}}^{4\times4}$ (left) and $\mathbf{Y}^{6\times6}$ (right).

B. Six Terminal Measurement And Processing

The six terminal measurement follows the procedure shown in earlier works and is briefly outlined here for convenience.

1. Measure the elements of $\mathbf{Y}^{6\times6}$ one-by-one, using the VNA with measurement and current sensor as described in [9].
2. Eliminate the effect of measurement cables from $\mathbf{Y}^{6\times6}$ using the transmission line method [16], similarly as for $\mathbf{Y}^{4\times4}$.
3. Merge the new $\mathbf{Y}^{6\times6}(\omega)$ with the frequency response $\mathbf{Y}_{\text{nom}}^{6\times6}(\omega)$ which is calculated from the transformer nominal data [23].
4. Modify the four matrix blocks of $\mathbf{Y}^{6\times6}$ by subtracting from each matrix column the column average, and from

This article has been accepted for publication in IEEE Transactions on Power Delivery. This is the author's version which has not been fully edited and content may change prior to final publication. Citation information: DOI 10.1109/TPWRD.2021.3098701

each row the row average [10]. This modified matrix is in the following denoted $\bar{\mathbf{Y}}^{6\times6}$.

Step 3 ensures that the data set defines a transformer with correct voltage ratio and short-circuit impedance characteristics at 50 Hz. The merging is done using first order filters so that the dataset smoothly changes from $\mathbf{Y}_{\text{nom}}^{6\times6}(\omega)$ to $\mathbf{Y}^{6\times6}(\omega)$ as the frequency is increased.

Step 4 enforces that each 3×3 block gets a zero sequence eigenvector with zero eigenvalue that is orthogonal with respect to the two other eigenvectors [10].

C. Combining Four-Terminal And Six-Terminal Measurements

It is reasonable to assume that the transformer is symmetrical with respect to the three HV terminals and three LV terminals. One implication is that application of a common voltage on all HV terminals and on all LV terminals give an identical current flow on all HV terminals and LV terminals, compliant with Step 4 above for creating $\bar{\mathbf{Y}}^{6\times6}$. Another implication is that an applied voltage on a neutral terminal will give an identical flow of current on all HV terminals and all LV terminals when those terminals are grounded.

With this assumption, the six-terminal matrix $\bar{\mathbf{Y}}^{6\times6}$ with partitions $\bar{\mathbf{A}}$, $\bar{\mathbf{B}}$, $\bar{\mathbf{C}}$, $\bar{\mathbf{D}}$ can be combined with the four-terminal matrix $\tilde{\mathbf{Y}}^{4\times4}$ from Section VI.A as shown in Fig. 20, giving $\mathbf{Y}^{8\times8}$. $\mathbf{1}_{m\times n}$ denotes a matrix of one's with dimension $m\times n$. $\mathbf{Y}^{8\times8}$. Further justifications and explanations of the procedure are given in Appendix B.

$$\mathbf{Y}^{8\times8} = \begin{array}{|c|c|c|c|}
\hline
\bar{\mathbf{A}} + \frac{\tilde{Y}_{11}^{4\times4}}{9}\cdot\mathbf{1}_{3\times3} & \bar{\mathbf{B}} + \frac{\tilde{Y}_{12}^{4\times4}}{9}\cdot\mathbf{1}_{3\times3} & \frac{\tilde{Y}_{13}^{4\times4}}{3}\cdot\mathbf{1}_{3\times1} & \frac{\tilde{Y}_{14}^{4\times4}}{3}\cdot\mathbf{1}_{3\times1} \\
\hline
\bar{\mathbf{C}} + \frac{\tilde{Y}_{21}^{4\times4}}{9}\cdot\mathbf{1}_{3\times3} & \bar{\mathbf{D}} + \frac{\tilde{Y}_{22}^{4\times4}}{9}\cdot\mathbf{1}_{3\times3} & \frac{\tilde{Y}_{23}^{4\times4}}{3}\cdot\mathbf{1}_{3\times1} & \frac{\tilde{Y}_{24}^{4\times4}}{3}\cdot\mathbf{1}_{3\times1} \\
\hline
\frac{\tilde{Y}_{31}^{4\times4}}{3}\cdot\mathbf{1}_{1\times3} & \frac{\tilde{Y}_{32}^{4\times4}}{3}\cdot\mathbf{1}_{1\times3} & \tilde{Y}_{33}^{4\times4} & \tilde{Y}_{34}^{4\times4} \\
\hline
\frac{\tilde{Y}_{41}^{4\times4}}{3}\cdot\mathbf{1}_{1\times3} & \frac{\tilde{Y}_{42}^{4\times4}}{3}\cdot\mathbf{1}_{1\times3} & \tilde{Y}_{43}^{4\times4} & \tilde{Y}_{44}^{4\times4} \\
\hline
\end{array}$$

Fig. 20. Establishing $\mathbf{Y}^{8\times8}$ from $\bar{\mathbf{Y}}^{6\times6}$ and $\tilde{\mathbf{Y}}^{4\times4}$.

D. Model Extraction

The eight-terminal matrix $\mathbf{Y}^{8\times8}$ is subjected to pole-residue modeling and passivity enforcement using the same technique as described in Section V.E. Fig. 21 shows the eigenvalues of $\mathbf{Y}^{8\times8}$ and of the admittance matrix associated pole-residue model. It is observed that the main features are well represented by the model.

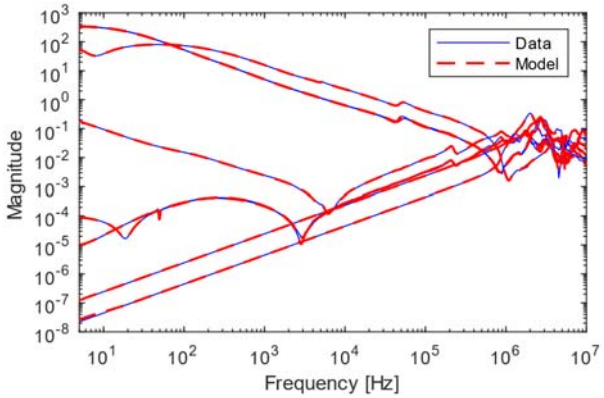

Fig. 21. Eigenvalues of $\mathbf{Y}^{8\times8}$.

E. Time domain Validation

The accuracy of the 8×8 model was verified by a number of time domain tests. Fig. 22 shows one test where the transformer is connected to resistors, with both neutrals open. A step voltage is applied to node "0" in the figure, and the voltage on node 0 is measured along with the voltage on terminals 1, 2, 4, 5, 7 and 8. The model is included in an EMT simulation with the same terminal conditions. Fig. 23 shows that the model gives an excellent reproduction of the measured voltage waveforms.

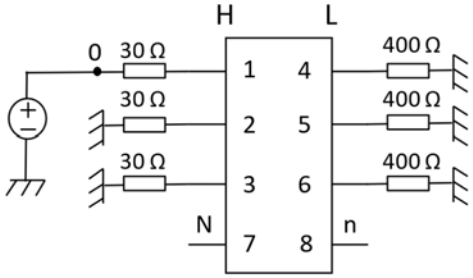

Fig. 22. Voltage excitation on HV side.

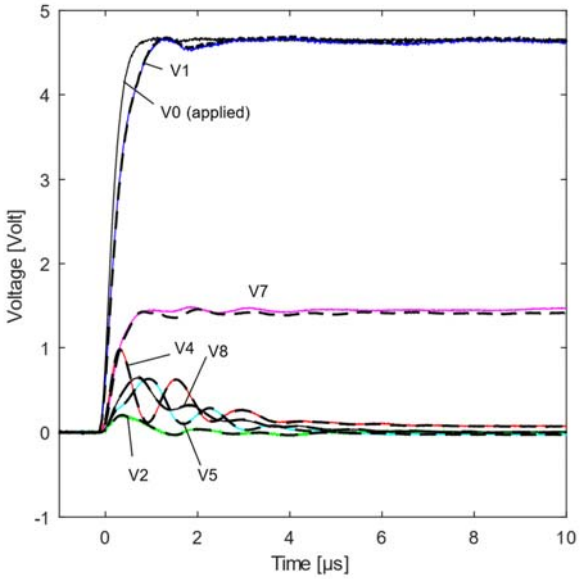

Fig. 23. Measured (solid traces) and simulated voltages (dashed traces).

This article has been accepted for publication in IEEE Transactions on Power Delivery. This is the author's version which has not been fully edited and content may change prior to final publication. Citation information: DOI 10.1109/TPWRD.2021.3098701

F. Comparison With Nominal Data

It is desirable that that transformer model has a reasonably accurate behavior also at nominal frequency. Table II compares the transformer's nominal data with those calculated by the model with the neutral points insulated from ground. It can be seen that the model reproduces the voltage ratio and short-circuit impedance with good accuracy. The good agreement is an effect of the merging with nominal data described in Section VI.B. The magnetizing current of the model is however unrealistic high, being 7.3% of the transformer nominal current.

TABLE II
VOLTAGE RATIO AND SHORT-CIRCUIT IMPEDANCE AT 50 HZ.

	Data sheet	8×8 Model
V_S/V_P	0.0209	0.0211
$(e_r + je_k)$ [%]	(1.7+j4.7)	(1.6+j4.9)

VII. TRANSFORMER TANK REFERENCE TERMINAL

The presented models make use of the transformer tank voltage as reference for ground. The transformer tank potential will however shift with respect to remote ground when a substantial current flows in the transformer local ground system. In such situation the model needs to be augmented such that the transformer tank becomes a reference terminal to which a grounding impedance can be connected. Such reference terminal is introduced by mathematical manipulation of the pole-residue model. The details of the manipulation was already shown in [15] and is therefore not repeated here.

VIII. DISCUSSION

In the case of transformers with a high voltage ratio, the capacitive asymmetry is important mainly for voltage transfer calculations from the HV-winding to the LV winding. The asymmetry is of less importance for voltage transfer calculations from the LV-side to the HV side because the capacitively coupled voltage is then small compared to the HV-side operating voltage.

IX. CONCLUSION

A new measurement-based approach has been developed for frequency-dependent transformer modeling that is capable of including the transformer neutral points as terminals, without having to make unwarranted assumptions about symmetry regarding the line and neutral ends. The availability of the terminals makes it possible to connect grounding impedances and surge protective devices to the neutral points.

Two pole-residue type models of a wye-wye connected transformer were developed: one four-terminal model with the HV and LV terminals bonded, and one eight-terminal model without such bondings. The four-terminal model is intended for lightning overvoltage studies where the overvoltages mainly occur as zero sequence voltages. The eight-terminal model is useful in general overvoltage studies.

APPENDIX A
MEASUREMENTS

A carefully designed measurement setup with associated calibration procedures is necessary for achieving the required accuracy. When performing the four-terminal measurements, the winding terminals are bonded on the HV and LV sides as shown in Fig. 24. On each side, the three terminals are bonded using a (straight) wire that connects the terminals. The bonded terminals and the neutral point are brought to a connection box by two separate coaxial cables. The cable screens are connected to an artificial ground plane on the transformer and to the measurement box chassis. The actual measurements are performed on the connection box which includes a built-in wide-band current sensor [9]. The VNA instrument, voltage probes and injection transformer are connected externally to the box. When performing six-terminal measurements, a total of six measurements cables are used. In both cases, the effect of the measurement cables are eliminated using the transmission line method in [24], thereby obtaining measurements that represent the transformer alone. Calibration is also used to eliminate the non-ideal frequency response of the current sensor and insertion impedance effects [25].

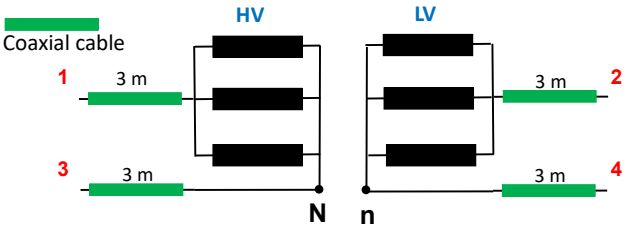

Fig. 24. Bonding of transformer terminals in four-terminal measurements.

APPENDIX B
MATRIX COMBINATION PROCEDURE

The rationale behind the procedure for combining the four terminal and a six terminal admittance matrices into an eight terminal matrix is the following. Consider the building of the upper left 3×3 part of $\mathbf{Y}^{8\times8}$ in Fig. 20. This submatrix $\mathbf{A}$ is built from two contributions, $\bar{\mathbf{A}}$ from $\mathbf{Y}^{6\times6}$, and element (1,1) from $\tilde{\mathbf{Y}}^{4\times4}$,

$$\mathbf{A} = \bar{\mathbf{A}} + \frac{\tilde{Y}_{11}^{4\times4}}{9} \tag{7}$$

$\mathbf{A}$ is associated with the 3×1 voltage and current vectors $\mathbf{v}$ and $\mathbf{i}$ at the first three terminals when the voltage is zero on all other terminals. The current response $\mathbf{i}$ from a general voltage application $\mathbf{v}$ can now be expressed as $\mathbf{i} = \mathbf{i}_1 + \mathbf{i}_2$ where

$$\mathbf{i}_1 = \bar{\mathbf{A}}[v_1 \quad v_2 \quad v_3]^T \tag{8a}$$

and

$$\mathbf{i}_2 = \frac{\tilde{Y}_{11}^{4\times4}}{9}\begin{bmatrix}1 & 1 & 1\\ 1 & 1 & 1\\ 1 & 1 & 1\end{bmatrix}[v_1 \quad v_2 \quad v_3]^T \tag{8b}$$

$\bar{\mathbf{A}}$ has one zero sequence eigenvector $\mathbf{t}_0 = [1 \quad 1 \quad 1]^T / \sqrt{3}$ whose eigenvalue is zero. This eigenvector is also orthogonal with respect to the two other eigenvectors. This implies that if one applies the voltages $\mathbf{v} = [1 \quad 1 \quad 1]^T$ to the HV terminals, the contribution from $\bar{\mathbf{A}}$ is $\mathbf{i}_1 = \mathbf{0}$ while the second contribution $\mathbf{i}_2$ is a zero sequence current vector $\mathbf{i}_2 = (\tilde{Y}_{11}^{4\times4} / 3)[1 \quad 1 \quad 1]^T$. Conversely, if the applied voltage **v** does not include any zero sequence component, the current response is given as $\mathbf{i}_1$ alone since $\mathbf{i}_2 = \mathbf{0}$. Also, the current response $\mathbf{i}_2$ does not include any zero sequence component, due to the aforementioned eigenvector orthogonality. It follows that the upper left 3×3 block of $\mathbf{Y}^{8\times8}$ as defined by (7) inherits the properties of $\tilde{\mathbf{Y}}^{4\times4}$ with zero sequence voltage excitations while it inherits the properties of $\mathbf{Y}^{6\times6}$ for voltage excitations that do not include zero common mode components. Similar reasoning can be made for the other matrix blocks of $\mathbf{Y}^{8\times8}$.

REFERENCES

[1] A. Greenwood, *Electrical transients in power systems*, John Wiley & Sons, 1991

[2] J. A. Martinez-Velasco, *Transient analysis of power systems: Solution techniques, tools and applications*, Wiley-IEEE, 2014.

[3] Technical Brochure 577A, "Electrical transient interaction between transformers and the power system. Part 1 – Expertise", CIGRE JWG A2/C4.39, April 2014.

[4] B. Gustavsen, C. Martin, A. Portillo, "Time domain implementation of damping factor white-box transformer model for inclusion in EMT simulation programs", *IEEE Trans. Power Delivery*, vol. 35, no. 2, pp. 464-472, April 2020.

[5] E. E. Mombello, A. Portillo and G. A. Diaz, "New state-space white-box transformer model for the calculation of electromagnetic transients," *IEEE Trans. Power Delivery*, doi: 10.1109/TPWRD.2020.3023824.

[6] Technical Brochure 39, "Guidelines for representation of network elements when calculating transients", CIGRE WG 33.02, 1990.

[7] A. Morched, L. Marti, and J. Ottevangers, "A high frequency transformer model for the EMTP," *IEEE Trans. Power Delivery*, vol. 8, no. 3, pp. 1615-1626, July 1993.

[8] Z. Zhongyuan, C. Yutong, L. Yupeng and L. Fangcheng, "High frequency circuit model of transformer windings based on frequency responses for VFTO studies,"*Third Int. Conf. on Electric Utility Deregulation and Restructuring and Power Technologies*, Nanjing, 2008, pp. 1528-1532.

[9] B. Gustavsen, "Wide band modeling of power transformers", *IEEE Trans. Power Delivery*, vol. 19, no. 1, pp. 414-422, Jan. 2004.

[10] B. Gustavsen, "Frequency-dependent modeling of power transformers with ungrounded windings", *IEEE Trans. Power Delivery*, vol. 19, no. 3, pp. 1328-1334, July 2004.

[11] A. Borghetti, A. Morched, F. Napolitano, C. A. Nucci and M. Paolone, "Lightning-Induced Overvoltages Transferred Through Distribution Power Transformers," *IEEE Trans. Power Delivery*, vol. 24, no. 1, pp. 360-372, Jan. 2009.

[12] T.A. Papadopoulos, A.I. Chrysochos, A.I. Nousdilis, G.K. Papagiannis, "Simplified measurement-based black-box modeling of distribution transformers using transfer functions", Electric Power Systems Research, vol. 121, 2015, pp. 77-88.

[13] D. Filipović-Grčić, B. Filipović-Grčić and I. Uglešić, "High-frequency model of the power transformer based on frequency-response measurements," *IEEE Trans. on Power Delivery*, vol. 30, no. 1, pp. 34-42, Feb. 2015.

[14] B. Gustavsen, A. Portillo, R. Ronchi, A. Mjelve, "High-frequency resonant overvoltages in transformer regulating winding caused by ground fault initiation on feeding cable", *IEEE Trans. Power Delivery*, vol. 33, no. 2, pp. 699-708, April 2018.

[15] B. Gustavsen, K. Longva, "Neutral point overvoltages in wye-wye connected distribution transformer caused by lightning current in low-voltage winding", *IEEE Trans. Power Delivery*, available online: ieeeXplore.

[16] B. Gustavsen, "Eliminating measurement cable effects from transformer admittance measurements", *IEEE Trans. Power Delivery*, vol. 31, no. 4, pp. 1609-1617, August 2016.

[17] B. Gustavsen, "Rational modeling of multi-port systems via a symmetry and passivity preserving mode-revealing transformation", *IEEE Trans. Power Delivery*, vol. 29, no. 1, pp.199-205, February 2014.

[18] B. Gustavsen and A. Semlyen, "Rational approximation of frequency domain responses by vector fitting", *IEEE Trans. Power Delivery*, vol. 14, no. 3, pp. 1052-1061, July 1999.

[19] B. Gustavsen, "Improving the pole relocating properties of vector fitting", *IEEE Trans. Power Delivery*, vol.21, no. 3, pp. 1587-1592, July 2006.

[20] D. Deschrijver, M. Mrozowski, T. Dhaene, and D. De Zutter, "Macromodeling of multiport systems using a fast implementation of the vector fitting method", *IEEE Microwave and Wireless Components Letters*, vol. 18, no. 6, pp. 383-385, June 2008.

[21] B. Gustavsen and A. Semlyen, "Enforcing passivity for admittance matrices approximated by rational functions", *IEEE Trans. Power Systems*, vol. 16, pp. 97-104, Feb. 2001.

[22] B. Gustavsen, "Passivity enforcement by residue perturbation via constrained non-negative least squares", *IEEE Trans. Power Delivery*, available online: ieeeXplore.

[23] B. Gustavsen, "A filtering approach for merging transformer high-frequency models with 50/60-Hz low-frequency models", *IEEE Trans. Power Delivery*, vol. 30, no. 3, pp. 1420-1428, June 2015.

[24] B. Gustavsen, "Eliminating measurement cable effects from transformer admittance measurements", *IEEE Trans. Power Delivery*, vol. 31, no. 4, pp. 1609-1617, August 2016.

[25] B. Gustavsen, "Removing insertion impedance effects from transformer admittance measurements", *IEEE Trans. Power Delivery*, vol. 27, no. 2, pp.1027-1029, April 2012.

BIOGRAPHY

Bjørn Gustavsen (M'94–SM'2003–F'2014) was born in Norway in 1965. He received the M.Sc. degree and the Dr. Ing. degree in Electrical Engineering from the Norwegian Institute of Technology (NTNU) in Trondheim, Norway, in 1989 and 1993, respectively. Since 1994 he has been working at SINTEF Energy Research where he is currently a Chief Research Scientist. He is also an adjunct Professor at NTNU, since 2020. His interests include simulation of electromagnetic transients and modeling of frequency dependent effects. He spent 1996 as a Visiting Researcher at the University of Toronto, Canada, and the summer of 1998 at the Manitoba HVDC Research Centre, Winnipeg, Canada. He was a Marie Curie Fellow at the University of Stuttgart, Germany, August 2001–August 2002.